J. metamorphic Geol., 2003, **21,** 439–453

Orthopyroxene–sillimanite–quartz assemblages: distribution, petrology, quantitative *P–T–X* constraints and *P–T* paths

D. E. KELSEY, R. W. WHITE AND R. POWELL
School of Earth Sciences, University of Melbourne, Victoria 3010, Australia (d.kelsey@pgrad.unimelb.edu.au)

ABSTRACT Granulite facies magnesian metapelites commonly preserve a wide array of mineral assemblages and reaction textures that are useful for deciphering the metamorphic evolution of a terrane. Quantitative pressure, temperature and bulk composition constraints on the development and preservation of characteristic peak granulite facies mineral assemblages such as orthopyroxene + sillimanite + quartz are assessed with reference to calculated phase diagrams. In NCKFMASH and its chemical subsystems, peak assemblages form mainly in high-variance fields, and most mineral assemblage changes reflect multivariant equilibria. The rarity of orthopyroxene–sillimanite–quartz-bearing assemblages in granulite facies rocks reflects the need for bulk rock X_{Mg} of greater than approximately 0.60–0.65, with pressures and temperatures exceeding *c.* 8 kbar and 850 °C, respectively. Cordierite coronas mantling peak minerals such as orthopyroxene, sillimanite and quartz have historically been used to infer isothermal decompression *P–T* paths in ultrahigh-temperature granulite facies terranes. However, a potentially wide range of *P–T* paths from a given peak metamorphic condition facilitate retrograde cordierite growth after orthopyroxene + sillimanite + quartz, indicating that an individual mineral reaction texture is unable to uniquely define a *P–T* vector. Therefore, the interpretation of *P–T* paths in high-grade rocks as isothermal decompression or isobaric cooling may be overly simplistic. Integration of quantitative data from different mineral reaction textures in rocks with varying bulk composition will provide the strongest constraints on a *P–T* path, and in turn on tectonic models derived from these paths.

Key words: cordierite; granulite; mineral reaction texture; NCKFMASH; *P–T* path.

Mineral abbreviations: orthopyroxene, opx; sillimanite, sill; quartz, q; garnet, g; cordierite, cd; kyanite, ky; K-feldspar, ksp; biotite, bi; muscovite, mu; corundum, crn; osumilite, osm; spinel, sp.; ilmenite, ilm; ilmenohematite, ilh; magnetite, mt; rutile, ru; hematite, hem; haemoilmenite, hi; perthite, pth; mesoperthite, mp; silicate, melt, liq; water, H_2O.

INTRODUCTION

An important aspect of metamorphic geology is the determination of vectors of the *P–T* path from mineral assemblages and reaction textures that provide insight into crustal processes. Qualitative and semiquantitative petrogenetic grids in simple model chemical systems approximating metapelitic rocks have paved the way to understanding the metamorphic evolution of granulite facies terranes. These include univariant reaction grids in FMAS (Hensen, 1971; Hensen, 1986; Waters, 1986; Hensen, 1987; Hensen & Harley, 1990), KFMAS (Grew, 1982), KFMASH (Grant, 1985; Hensen & Harley, 1990; Audibert *et al.*, 1995; Carrington & Harley, 1995; McDade & Harley, 2001), FMASTO (Powell & Sandiford, 1988; Guiraud *et al.*, 1996), KFMASTO (Sandiford *et al.*, 1987) and KFMASHTO (Clarke *et al.*, 1989; Clarke & Powell, 1991). Many authors have interpreted reaction textures in aluminous and magnesian granulite facies metapelites in terms of such grids (e.g. Lal *et al.*, 1987; Kamineni & Rao, 1988; Harley *et al.*, 1990; Dasgupta *et al.*, 1995; Guiraud *et al.*, 1996; Ouzegane & Boumaza, 1996; Mouri *et al.*, 1996; Harley, 1998a; Harley, 1998b; Harley, 1998c), using topological constraints to derive vectors of the *P–T* path. However, mineral reaction textures are commonly the consequence of higher-variance (continuous) reaction processes (e.g. Stüwe & Powell, 1995; White *et al.*, 2002) that are difficult to depict with univariant reaction grids. Moreover, the effect of bulk composition and open system processes on mineral assemblage development are difficult to assess with a qualitative approach.

Difficulty in qualitatively deriving a *P–T* path on the basis of mineral reaction textures is reflected by two commonly inferred retrograde *P–T* paths for granulite facies terranes: (1) isothermal decompression (ITD); and (2) isobaric cooling (IBC) paths. Quantitative *P–T* diagrams in the form of calculated pseudosections potentially provide a more rigorous means of determining the retrograde *P–T* evolution of granulite facies terranes (White *et al.*, 2001; White *et al.*, 2002; White & Powell, 2002; Johnson *et al.*, 2003). Calculated pseudosections can be used to integrate information such as the preserved mineral assemblage(s), bulk composition of the equilibration volume (*X*)

(changes in) relative mineral proportions, mineral chemistry and inferred reaction texture development (e.g. Stüwe & Powell, 1995). Thus *P–T* paths accounting for the development of high-variance mineral assemblages may be explored in detail. Moreover, the graphical depiction of petrologically inferred equilibrium mineral assemblages in *P–T–X* space removes some of the problems associated with retrograde resetting of mineral compositions that hamper most 'classic' geothermobarometric techniques, i.e. based on cation exchange and/or net-transfer reactions.

Orthopyroxene–sillimanite–quartz assemblages are rare and characteristic of deep-crustal ultrahigh-temperature (UHT) metamorphism of pelitic and impure-quartzitic bulk compositions (e.g. Harley, 1998a; Harley, 1998c). As the assemblage is confined to extreme conditions of crustal metamorphism, it, and its related reaction textures, are potentially useful for delineating the metamorphic conditions of a granulite facies terrane. The summary of occurrences of orthopyroxene–sillimanite–quartz-bearing assemblages in Table 1 provides a framework in which to investigate the *P–T–X* constraints on the development of this granulite facies assemblage. Calculated *T–X* and *P–T* pseudosections in the NCKFMASH and KFMASH model metapelitic systems are presented for the purpose of: (1) exploring quantitatively the *P–T* and particularly compositional (*X*) restrictions on the development of peak orthopyroxene + sillimanite + quartz; (2) factors leading to the preservation of (peak) granulite facies assemblages; and (3) providing a basis for considering how effectively a preserved mineral reaction texture is able to define dP/dT of the retrograde *P–T* path, citing examples of orthopyroxene–sillimanite–quartz-bearing assemblages from the literature. It will be demonstrated that the common interpretation of ITD or IBC paths from a mineral reaction texture neglects a wide range of other possibilities.

One of the difficulties in metamorphic geology is deciphering whether a *P–T* path reflects a composite path with segments recording temporally unrelated metamorphic episodes. Some high-temperature granulite facies terranes have been interpreted as recording prolonged and complex tectonothermal histories, with repeated granulite facies events apparently preserved (e.g. Sarkar *et al.*, 1981; Droop, 1989; Harley & Fitzsimons, 1991; Rickers *et al.*, 2001; Kelly *et al.*, 2002). For the purposes of simplifying the following discussion, it is assumed that polymetamorphism has not occurred.

ORTHOPYROXENE–SILLIMANITE–QUARTZ OCCURRENCES

Quartz-bearing orthopyroxene–sillimanite assemblages are documented from regional granulite facies terranes worldwide (Table 1). *P–T* paths for rocks in which these assemblages occur have been derived on the basis of mineral textural evidence in conjunction with qualitative and/or semiquantitative univariant reaction grids and 'classic' thermobarometry. Cordierite moats mantling interpreted peak mineral assemblages including orthopyroxene, sillimanite and quartz are common (Fig. 1a). From this and other mineral reaction textures, ITD *P–T* paths passing down-pressure between the spinel–biotite-absent and quartz–biotite-absent invariant points of Hensen's (1971, 1986) grids are typically inferred (Table 1, excepting Algeria). Less commonly, higher-temperature/lower-pressure sapphirine + quartz assemblages, rather than cordierite, postdate the development of peak or prograde orthopyroxene + sillimanite + quartz (e.g. Hoggar, Algeria; Bertrand *et al.*, 1992; Guiraud *et al.*, 1996; Mouri *et al.*, 1996; Ouzegane & Boumaza, 1996). In contrast, orthopyroxene–sillimanite–quartz assemblages may occur as coronae and/or symplectites postdating the development of sapphirine–quartz and/or spinel–quartz assemblages (Fig. 1b,1c). Further retrograde reaction postdating orthopyroxene–sillimanite–quartz, in the form of kyanite and/or cordierite, may occur. For these occurrences IBC *P–T* paths are typically inferred (Table 1). Indeed, sapphirine–quartz-bearing assemblages appear to be confined to IBC terranes, with Algeria being an exception. It will be shown that invoking ITD and IBC paths to explain the development of such mineral reaction textures may be overly simplistic.

Experimental investigations (e.g. Annersten & Seifert, 1981; Audibert *et al.*, 1995; Carrington, 1995; Carrington & Harley, 1995) have indicated minimum conditions of around 900–1000 °C and ≥ 8–9 kbar are required for the generation of orthopyroxene + sillimanite + quartz assemblages, supported by mineral equilibria modelling (White *et al.*, 2001; White *et al.*, 2002). While most peak *P–T* estimates in Table 1 are consistent with these stability limits, several estimates do lie outside (Grew, 1980; Harris & Holland, 1984; Avakyan & Dmitriyeva, 1985; Lal *et al.*, 1987; Kamineni & Rao, 1988). Difficulties in estimating peak *P–T* conditions for natural granulite facies assemblages are largely related to: (1) retrograde resetting of mineral compositions; (2) necessity to input *P* to derive *T* and vice versa with 'classic' geothermobarometry; (3) a potentially large *P–T* range over which a peak assemblage may be stable; (4) univariant reaction grids that do not account for bulk composition; and (5) a previous inability to calculate phase diagrams in geologically realistic chemical systems. In addition to these factors, each orthopyroxene–sillimanite–quartz-bearing terrane has likely experienced differing tectonothermal settings.

P–T–X CONTROLS ON METAMORPHIC ASSEMBLAGES

Pseudosections represent a two-dimensional slice of *P–T–X* space, and allow one to investigate the role of two variables (*P* or *T* or *X*) with the third fixed. The pseudosections presented here were calculated using THERMOCALC v3.0 (26 October 1999 update of Powell & Holland, 1988, internally consistent dataset, th dpdata1 +,2 +, created 19 September 1999) for the model chemical systems Na_2O-CaO-K_2O-FeO-MgO-Al_2O_3-SiO_2-H_2O (NCKFMASH) and K_2O-FeO-MgO-Al_2O_3-SiO_2-H_2O (KFMASH). NCKFMASH calculations used the mineral and liquid/melt activity-composition models and non–ideal interaction parameters of White *et al.* (2001). KFMASH calculations used Na-Ca-free derivatives of the same activity-composition models. Feldspars are modelled as ternary in the NCKFMASH system.

To investigate the roles of *X*, *P* and *T* on the development of orthopyroxene–sillimanite–quartz-bearing assemblages a series of T–X_{Mg} and T–X_{Al} pseudosections are presented at 9 and 10 kbar (Fig. 2), in addition to related *P–T* pseudosections (Fig. 3). The bulk compositions are adapted from the 'average pelite' composition in White *et al.* (2001), differing here

Table 1. Summary of orthopyroxene–sillimanite–quartz occurrences, subdivided into localities interpreted to record ITD (typically clockwise) and IBC (typically anticlockwise) *P–T* paths. Both peak and retrograde orthopyroxene–sillimanite–quartz assemblages occur. Retrograde cordierite is common. Preserved $X_{Mg,opx}$ may be considered as a first-pass estimation of $X_{Mg,bulk}$ for the mineral assemblage bulk composition. y(opx) ≡ $X_{Al,M1,opx}$ and $X_{Mg,opx}$ values are maxima and minima, respectively, as Fe^{3+} is not considered. Other abbreviations: OM = oxide mineral, ITD = isothermal decompression, IBC = isobaric cooling, ACW = anticlockwise, Retr. Minerals = retrograde minerals, Peak = peak *P–T* estimate in kbar and °C. Invariant points in [ ] refer to the Hensen (1971,1986,1987) FMAS univariant reaction grids.

Label	Location	Peak Assemblage	Retr. Minerals	Inferred *P-T* path	Peak (*P* kbar, *T*°C)	OM	y(opx)	X(Mg,opx)
"Isothermal decompression" and/or clockwise terranes								
HH84	Beitbridge, Limpopo Belt, Zimbabwe	?Prograde ky. Opx+sill+q+?bi	cd	near-ITD	≤5, 750±50	?	0.14	73
AD85	Kola Peninsula, Russia	opx+sill+q+ksp	1) sa+q, 2) cd	?	7.55 , 800	mt	0.16	73
H90	Forefinger Point, east Antarctica	opx+sill+q+ksp	cd	initial ITD between [sp bi] and [q bi]	10±1.5, 950±50	-	0.15	79
B92	In Ouzzal, Hoggar, Algeria,	q+opx+sill+g	1) sa+q, 2) g+sa+q, 3) cd	isobaric heating, then decompressional cooling	10±1.5, 970±70	mt	0.16	79, 82
G96	In Ouzzal, Hoggar, Algeria,	1) g+q, 2) g+q+opx+sill	1a) opx+sa+q, 1b) opx+sill 1c) sp+sa+ru+q, 2) sa+q	?	≥9, ≥1000	ru	0.17	74-79
M96	Ihouhaouene, Hoggar, Algeria	opx+sill+q+ksp. Peak bi	cd	initial ITD	≥10, ≥990	ru?	*c.* 0.18	*c.* 70
OB96	In Hihaou, Algeria	1) g+q, 2) opx+sill+g+pth+bi+q	1) opx+sill, 2) g+sa+q+bi; cd moats	ITD between [sp bi] and [opx bi]	10±1.5, *c.*1050	ru	0. 21	67-80
MI97	Lutzow-Holm Bay, east Antarctica	opx+sill±q	Prograde ky; cd	ITD between [sp bi] and [q bi]	*c.* 11, 1000	?	?	?
H98	Rauer Group, east Antarctica	opx+sill+q	cd	ITD between [sp bi] and [q bi]	12, 1050	-	*c.* 0.15	76
KS99	Hakurutale, Sri Lanka	1) g+q, 2) g+q+opx+sill+pl	1) opx+sill±pl, 2) cd	ITD between [sp bi] and [q bi]	9-9.2, 830	ru	0.13	79
"Isobaric cooling" and/or anticlockwise terranes								
MT71	Wilson Lake, Labrador, Canada	sa+q+mt+pl	opx+sill+ksp. Retrograde ky	IBC	≥11, ≥1100	Ti-mt	?	65-70
LM72	Wilson Lake, Labrador, Canada	1) sa+q, 2) opx+sill+?q	1) opx+sill, 2) cd	?	≥7, ≤1060	Ti-hem	?	*c.* 83
E80	Enderby Land, east Antarctica	sa+q	opx+sill; later cd	IBC	?	ru, ?mt	0.18	70
G80	Enderby Land, east Antarctica	sa+q	opx+sill	ACW	7±1, 900±30	ru	0.19	74-90
G82	Enderby Land, east Antarctica	osm+sa+q+pl	opx+sill	ACW	8-9, 900-1000	ru±ilm	0.17	92-93
S85	Enderby Land, east Antarctica	1) sa+q+mp+opx+ru, 2) sill+opx+mp+q+ru	1a) g+sill, 1b) opx+sill+crn, 2) g+bi	IBC	8-10, 850-1000	ru	?	*c.* 70-75
L87	Paderu, Eastern Ghats, India	1) sp+q+osm, 2) sa+q+osm, 3) opx+sill+q+osm	1) opx+sill, 2) opx+sill, cd moats, 3) opx+sill = g+q	ACW through [cd bi] and just above [sp bi]	6.5±0.7, 900±60	ru,ilm,ilh	0.20	66
S87	Labwor Hills, Uganda	1) sa+q+cd+ilh+mt, 2) sp+q+cd	1) opx+sill, 2) opx+sill	ACW, near-IBC	7-9, *c.* 1000	ilh, mt	0.23	65
CG88	Wilson Lake, Labrador, Canada	sa+q+mt+hem+ilm+mp	opx+sill	initial IBC, later ITD	≥10, *c.* 900	mt,hem,ilm	0.20	80
KR88	Vizianagaram, Eastern Ghats, India	1) sa+q, 2) sp+q	opx+sill; later cd	ACW with initial IBC	≥6, ≥850	mt	0.11	64
S90	Anantagiri, Eastern Ghats, India	1) sa+q+?cd, 2) sp+q+cd	opx+sill+g+q; later cd	IBC, then decompression	8.3, ≥950	ru±ilm	0.16	69
B99	South Harris, NW Scotland	sa+opx+sill+q	sa+q = opx+sill/ky; sill predates ky; later cd	ACW down-T, UP-pressure	10-12, 950-930	?ru	0.18	78
B00	Sunkarametta, Eastern Ghats, India	1) sa+q, 2) sp+q	1) opx+sill, 2) opx+sill+mt	ACW near-IBC	9, *c.* 950	ilm+mt, later ru	0.16	68
DMF00	Barro Alto Complex, Brazil	1) sp+q+hem/ilm, 2) sp+cd+ru+?q	1) opx+sill, 2) opx+sill+q later ky	ACW near-IBC	*c.* 7.9, *c.* 980	ru+ilh, hi	0.21	52-65
M02	Anapolis-Itaucu Complex, Brazil	sa+q+g+opx	opx+sill	initial near-ITD, then near-IBC	>10, 1030-1150	ru	0.25	68-69

HH84 = Harris & Holland (1984); AD85 = Avakyan & Dmitriyeva (1985); H90 = Harley *et al.* (1990); B92 = Bertrand *et al.* (1992); G96 = Guiraud *et al.* (1996); M96 = Mouri *et al.* (1996); OB96 = Ouzegane & Boumaza (1996); MI97 = Motoyoshi & Ishikawa (1997); H98 = Harley (1998b); KS99 = Kriegsman & Schumacher (1999); MT71 = Morse & Talley (1971); LM72 = Leong & Moore (1972); E80 = Ellis *et al.* (1980); G80 = Grew (1980); G82 = Grew (1982); S85 = Sandiford (1985); L87 = Lal *et al.* (1987); S87 = Sandiford *et al.* (1987); CG88 = Currie & Gittins (1988); KR88 = Kamineni & Rao (1988); S90 = Sengupta *et al.* (1990); B99 = Baba (1999); B00 = Bose *et al.* (2000); DMF00 = deMoraes & Fuck (2000); M02 = Moraes *et al.* (2002).

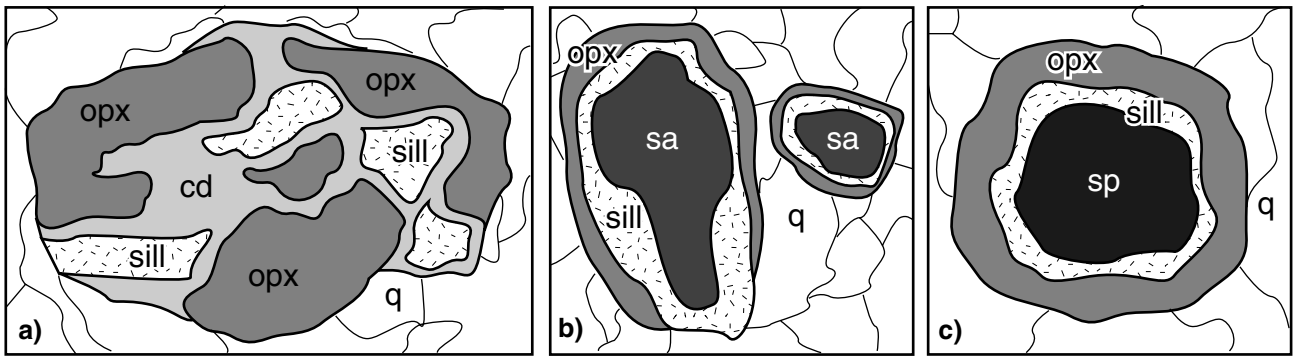

Fig. 1. Schematic examples of common textures involving orthopyroxene–sillimanite–quartz in UHT quartz-bearing metapelitic granulites. (a) Retrograde cordierite coronas mantling orthopyroxene and sillimanite. This texture is typically interpreted as a product of near-ITD. Sillimanite is rarely left in contact with quartz, whereas orthopyroxene-quartz contacts are more common. (b) Sapphirine + quartz mantled by retrograde sillimanite and orthopyroxene. Sillimanite is in contact with sapphirine in all reported cases. (c) Spinel + quartz mantled by retrograde sillimanite and orthopyroxene. Spinel in these cases is typically stabilised by minor components such as Fe^{3+}, Cr and/or Zn. Textures (b) and (c) are typically attributed to IBC or anticlockwise *P–T* paths.

also by the explicit inclusion of silica in a quantity to quartz-saturate the orthopyroxene-sillimanite assemblages. The H_2O content for Figs 2 and 3 is chosen such that the respective bulk compositions are just water-saturated at the solidus. Bulk compositions are expressed as molar percent. The topology of ferromagnesian phase relations is controlled by the KFMASH subsystem (Figs 2, 3; White *et al*., 2001).

Figure 2 reveals that common granulite facies assemblages such as garnet + sillimanite + quartz + liquid and garnet + orthopyroxene + quartz + liquid are produced by a range of more iron-rich bulk compositions (X_{Mg} 0–0.6; Fig. 2a–d). The only assemblage common to both Fig. 2(a,b) above *c* 860 °C is orthopyroxene + sillimanite + quartz + liquid/melt (± garnet), for which strict compositional limits have not been previously explored. From these diagrams, orthopyroxene–sillimanite–quartz-bearing assemblages require NCKFMASH bulk compositions more magnesian than X_{Mg} of 0.60–0.65 with $T \geq 860$ °C. *P–T* pseudosections (Fig. 3a,c,d) show orthopyroxene–sillimanite–quartz stability is restricted to $P \geq 8.0$–8.5 kbar. The presence of Na and Ca serve to stabilise orthopyroxene–sillimanite–quartz assemblages *c*. 20–30 °C down-temperature from KFMASH (compare Fig. 2b,d & 3a,b). In addition, the upper pressure limit of orthopyroxene–sillimanite–quartz stability increases with increasing X_{Mg} (compare Fig. 3a,c). At $X_{Mg} = 0.6$ (Fig. 2a,b), and with increasing pressure (Fig. 3a,d), $A/AFM = Al_2O_3/(Al_2O_3 + FeO + MgO)$ controls which of sillimanite or orthopyroxene remains stable (or alternatively destabilises first) for a given bulk composition.

$T–X_{Al}$ pseudosections (Fig. 2e,f) indicate that for $A/AFM \leq 0.45$ (in this case), the more aluminous a bulk composition is, the less magnesian it needs to be to develop orthopyroxene–sillimanite–quartz-bearing assemblages. That is, orthopyroxene–sillimanite–quartz-bearing assemblages expand to lower A/AFM values with increasing X_{Mg} (but still appear at more or less the same temperature).

The rarity of orthopyroxene–sillimanite–quartz-bearing assemblages in nature is a feature of bulk composition. Highly magnesian bulk rock compositions are volumetrically rare in nature (e.g. Chinner & Sweatman, 1968), commonly outcropping on only very localised scales (cm-m) within regional granulite terranes (see references in Table 1). It has been proposed that highly magnesian bulk compositions may represent residual bulk compositions (e.g. Lal *et al*., 1978; Droop & Bucher-Nurminen, 1984; Raith *et al*., 1997) developed as a consequence of the extraction of melt rich in silica and iron. Although Fe does have a greater affinity for melt than Mg, very little Fe and Mg partition into melt (much less than 1%). Hence the cumulative effect on the bulk $X_{Mg,residue}$ would be minor, resulting in only a slight Mg-enrichment. This point can be demonstrated by comparing the near-identical bulk X_{Mg} of compositions used in Figs 3(c) and 4, where Fig. 4 represents an illustrative residual bulk composition following two melt loss 'events' from the composition of Fig. 3(c) (using logic of White & Powell, 2002). In other words, highly magnesian assemblages must source from protoliths enriched in magnesium with respect to iron. There are few inferred UHT terranes without orthopyroxene–sillimanite–quartz assemblages (see Harley, 1998c), primarily because UHT terranes are recognised on the basis of assemblages (e.g. orthopyroxene–sillimanite–quartz, sapphirine-quartz, osumilite) that are largely restricted to magnesian rocks. Therefore the apparent rarity of UHT terranes may in part reflect the rarity of magnesian rocks (e.g. $X_{Mg} = 0.65$) rather than the ability of continental crust to achieve extreme temperature conditions (Pattison *et al*., 2003).

High-variance fields (variance, v = 3–6) dominate the NCKFMASH and KFMASH *P–T*, $T–X_{Mg}$ and $T–X_{Al}$ pseudosections. Consequently, calculations in

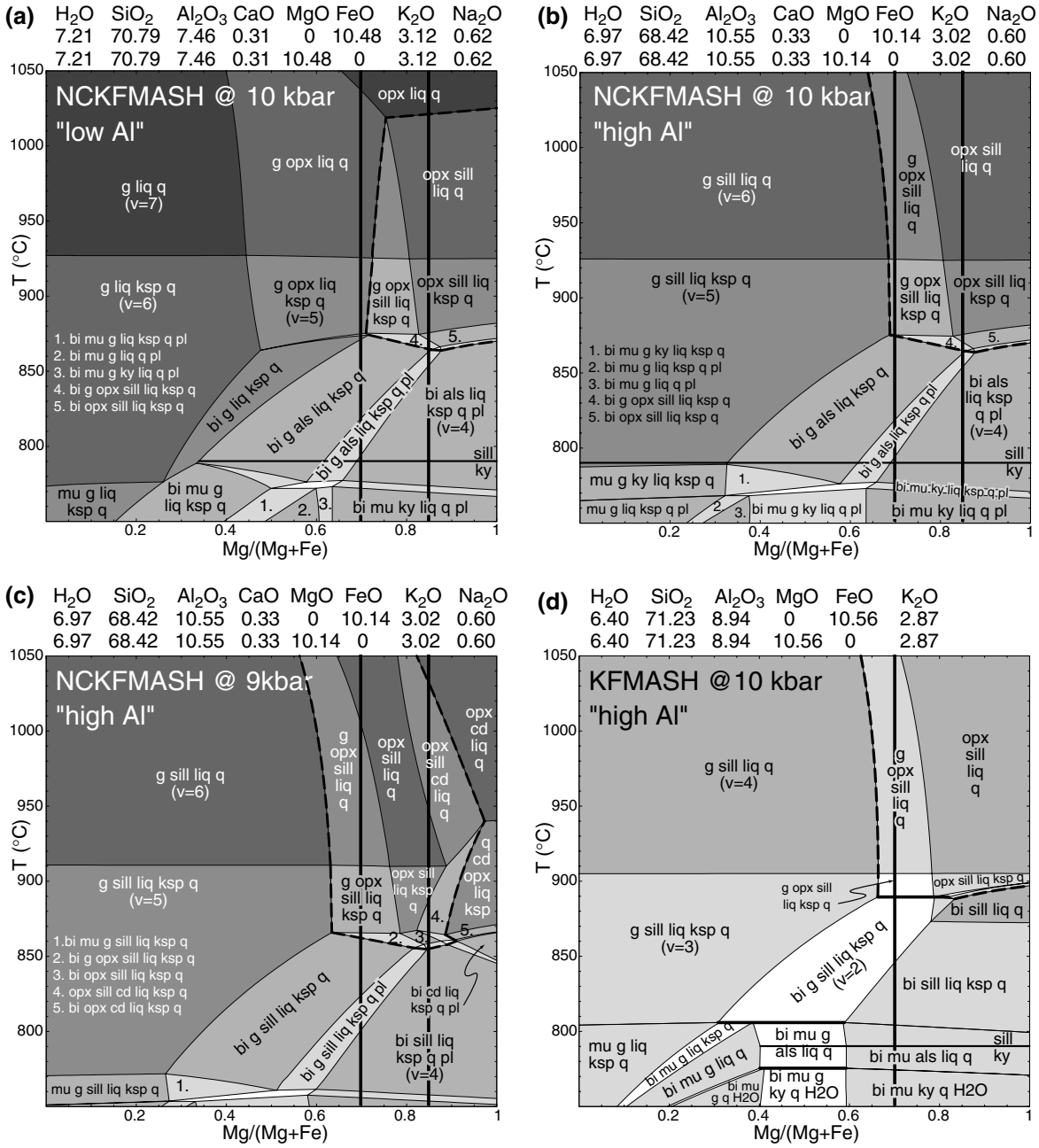

Fig. 2. T–X_{Mg} and T–X_{Al} pseudosections for different $Al_2O_3/(Al_2O_3 + FeO + MgO)$ and $MgO/(MgO + FeO)$ bulk compositions in a closed metapelitic system in NCKFMASH and KFMASH. Assemblage variance, v, is indicated in the fields. Stability of orthopyroxene–sillimanite–quartz-bearing assemblages is indicated by bold dashed lines. An isobaric prograde heating path is represented by moving upwards along any vertical line of fixed composition in pseudosections (a)–(f). Phase relations = 1000–1050 °C are likely to be affected by the presence of sapphirine. (a) T-X_{Mg} pseudosection at 10 kbar for 'low Al' bulk composition. Above *c*. 875 °C garnet-orthopyroxene assemblages occur at $X_{Mg} = 0.7$. Lower A/AFM will expand orthopyroxene + garnet + quartz + liquid stability to lower X_{Mg}. Given the abundance of orthopyroxene-garnet-quartz-bearing assemblages in granulite facies terranes, the bulk composition is close to the upper limit of Al content that will generate this assemblage. (b) T–X_{Mg} pseudosection at 10 kbar for 'high Al' bulk composition. The stability of orthopyroxene–sillimanite–quartz assemblages is expanded to slightly less magnesian compositions relative to (a). (c) T–X_{Mg} pseudosection at 9 kbar for 'high Al' bulk composition. In highly magnesian compositions ($X_{Mg} \geq 0.8$) the stability of cordierite elevates to = 9 kbar. (d) KFMASH T–X_{Mg} pseudosection at 10 kbar for comparison with (b). KFMASH provides the topological structure of ferro-magnesian relationships in larger systems. Orthopyroxene–sillimanite–quartz assemblages are stable to lower T in NCKFMASH. (e) and (f) T–X_{Al} pseudosections at 10 kbar, $X_{Mg} = 70$ and 85, respectively. At 10 kbar, bulk compositions less aluminous than *c*. 0.45 will only develop orthopyroxene–sillimanite–quartz assemblages at $X_{Mg} = 0.70$. Vertical lines at fixed composition on the pseudosections represent compositions at which P–T pseudosections of Fig. 3 are drawn. An isobaric prograde heating path is represented by moving upwards along any vertical line of fixed composition in pseudosections (a) to (f).

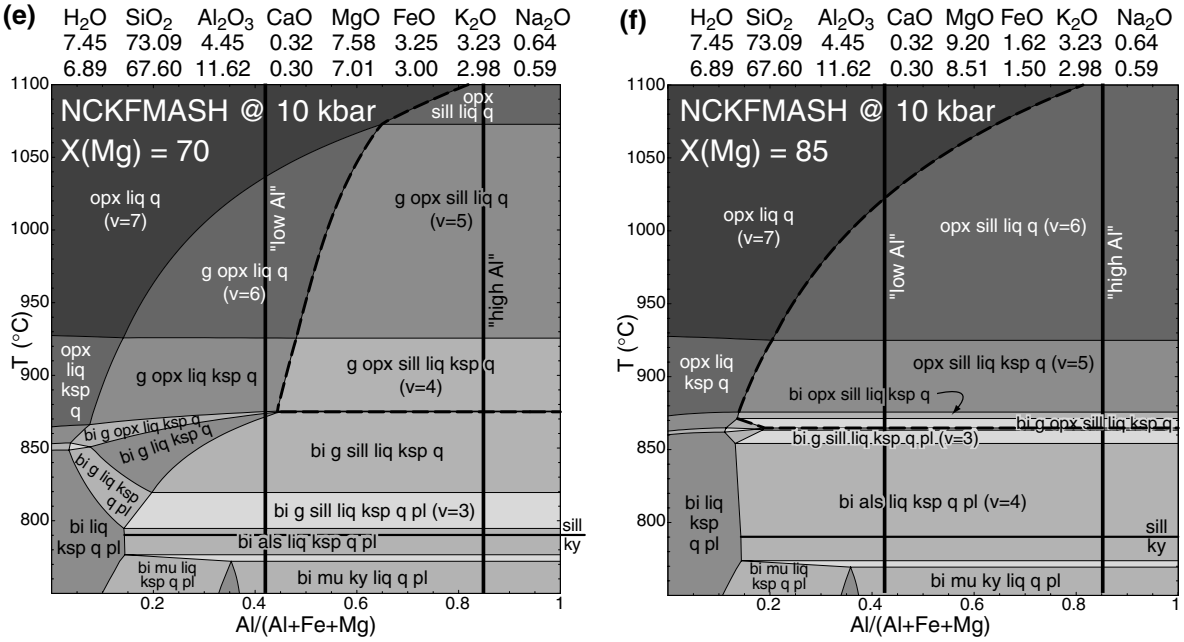

Fig. 2. (*Cont'd*).

KFMASH and NCKFMASH predict that metamorphic assemblage development is largely the result of high-variance processes, and not univariant or low-variance processes. The presence of components not included in the presented pseudosections (e.g. Ti, Fe^{3+}, Cr, Zn) are known to enhance the stability of minerals such as biotite and spinel (e.g. Peterson *et al.*, 1991; Hensen & Osanai, 1994; Guiraud *et al.*, 1996; Nair & Chacko, 2002; White *et al.*, 2002). Therefore extra, variance-increasing, components may cause the (?significant) displacement of fields in *P–T* space. Hence one should be aware of the implications of interpreting mineral reaction textures (e.g. biotite-bearing, spinel-quartz) within chemical systems that may be (far) removed from geologically realistic systems.

PRESERVATION OF GRANULITE FACIES MINERAL ASSEMBLAGES

Microstructural development in metamorphic rocks is a function of the mobility of elements through chemical and physical diffusion processes (e.g. Spear, 1993; Pattison & Bégin, 1994; Stüwe, 1997; Brown, 2002). The preservation of high-grade assemblages at the Earth's surface indicates that kinetic processes acting during the prograde and peak evolution are retarded significantly during the retrograde evolution. The preservation of peak metamorphic minerals that are incompletely consumed by coronae and symplectites is common in granulites. In addition, granulite facies rocks commonly contain several compositional domains, each having different mineral assemblages (Stüwe, 1997). Temperature, melt distribution, dP/dt and dT/dt place important constraints on element availability and mobility and hence effective bulk compositions and volumes of equilibration. With decreasing temperature during retrograde metamorphism, the kinetics of chemical and physical diffusion decrease exponentially, thus limiting the continued evolution of an equilibrium mineral assemblage and/or reaction texture (e.g. Stüwe, 1997). A general lack of retrogression of high-grade assemblages in granulite facies rocks was first suggested by Fyfe (1973a,b) to be related to open system processes, specifically the dehydration of the equilibration volume by removal of a hydrous component, melt/liquid. While early investigations were mainly qualitative (e.g. Powell, 1983; Waters, 1988; Powell & Downes, 1990), this has since been strongly supported in a quantitative manner by equilibrium thermodynamic calculations (e.g. White *et al.*, 2001; White *et al.*, 2002; White & Powell, 2002). Melt loss is aided and/or driven by deformation (e.g. Wickham, 1987; Hand & Dirks, 1992; Brown, 1994; Sawyer, 1994; Brown *et al.*, 1995; Brown & Rushmer, 1997; Rutter, 1997; Brown & Solar, 1998; Sawyer *et al.*, 1999). As the gneissic framework commonly remains intact (Vanderhaeghe, 2001) it is reasonable to assume that melt loss, incorporating the scale of a mineral reaction texture, primarily takes place progressively (Sawyer, 1994; Vanderhaeghe, 2001) to peak metamorphic conditions as major melting steps are crossed (White & Powell, 2002), and while pervasive ductile deformation is still most likely operating. Furthermore, a

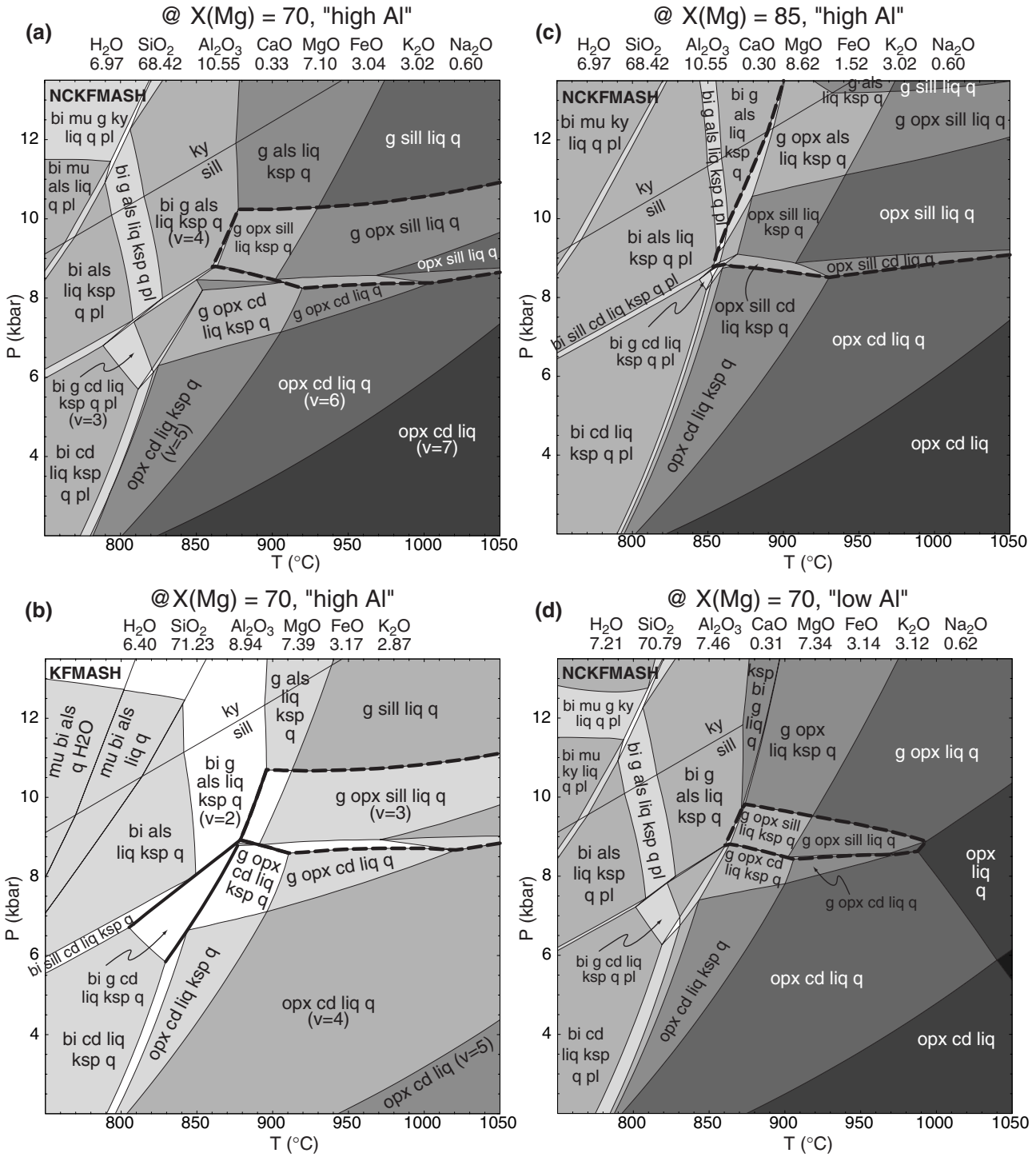

Fig. 3. *P–T* pseudosections for different $Al_2O_3/(Al_2O_3 + FeO + MgO)$ and $MgO/(MgO + FeO)$ bulk compositions in a closed metapelitic system. Field variance is indicated in (a) and (c). Stability of orthopyroxene–sillimanite–quartz-bearing assemblages is indicated by bold dashed lines. The amount of Na_2O and CaO is such that plagioclase reacts out below prior to the development of orthopyroxene–sillimanite–quartz assemblages. Quartz reacts out in the bottom right-hand corner of the pseudosections. The stability of garnet becomes limited to higher pressures with increasing X_{Mg}. (a) (c) and (d) NCKFMASH pseudosections corresponding to bulk compositions given by vertical lines in Fig. 2. (b) KFMASH *P–T* pseudosection for comparison with (a). Univariant reactions are highlighted in bold.

valid assumption is that equilibration and hence texture development is sufficiently rapid while a mobile phase such as melt is still present within the equilibration volume of a rock mass (White & Powell, 2002). If substantial melt loss has occurred, there may be insufficient H_2O (component) remaining in the equilibration volume to allow a high degree of retrogression (Brown, 2002). That is, H_2O removed with the melt is likely to be more important than retrograde reaction kinetics (analogous to Rubie, 1986; Ashworth, 1993; Yund, 1997; Guiraud *et al.*, 2001), despite the high temperature that may still prevail. The influence of each of these two variables is likely to be additionally controlled by dP/dt and dT/dt, about which pseudosections offer no information. Therefore, if open system processes involving melt liquid are inferred to have occurred, Figs 2 and 3 will unfortunately not be (directly) applicable for interpreting, for example, the retrograde history.

Assessing the retrograde evolution of granulite facies rocks with calculated phase diagrams must account for the effect of melt loss on bulk composition. A bulk composition modified through melt loss will result in the stability of high-grade assemblages expanding to lower pressure and temperature, changing the subsolidus phase topology (Fig. 4; White & Powell, 2002). Additionally, melt loss elevates the solidus temperature (particularly the biotite-solidus; compare Figs 3b and 4). Hence large amounts of melt loss may result in the solidus being crossed whilst the rock is still at elevated temperatures above the 'normal' solidus.

In terms of reading an *individual* pseudosection, the disappearance of melt/liquid from an equilibrium mineral assemblage field (e.g. Fig. 4) implies that the remaining melt in the equilibration volume has crystallized. The growth of cordierite to lower pressure and biotite to lower temperature in Fig. 4 therefore coincides with the final crystallisation of melt, replacing melt as the hydrous phase in the assemblage. In Fig. 4 the solidus is represented by two narrow NCKFMASH quadrivariant (v = 4) fields; the near-horizontal orthopyroxene + sillimanite + K-feldspar + cordierite + quartz + liquid field, and the near-vertical orthopyroxene + sillimanite/kyanite + K-feldspar + biotite + quartz + liquid field. Each of these narrow quadrivariant fields consist of closely spaced mineral proportion contours. Such fields may therefore be associated with extensive reaction and microstructural modification, depending additionally on the cooling rate. Importantly, the solid peak mineral assemblage will commonly *remain* part of the stable assemblage below the solidus, as also indicated in Fig. 4 by orthopyroxene–sillimanite–quartz-bearing assemblages both above and below the solidus. Thus it may be incorrect to conclude that orthopyroxene, sillimanite and quartz are in disequilibrium with respect to each other and cordierite or biotite during retrograde metamorphism.

Estimation of peak *P–T* conditions

The estimation of 'peak' (i.e. maximum preserved) *P–T* conditions is primarily based on the preservation of coarse-grained, porphyroblastic and/or prismatic minerals that are interpreted as constituting part of the peak mineral assemblage. Mineral resetting during retrograde metamorphism and/or cooling is typically decoupled (e.g. Fe-Mg diffuse faster than Al and Si; O'Hara, 1977; Frost & Chacko, 1989; Anovitz, 1991; Fitzsimons & Harley, 1994; Pattison & Bégin, 1994; Pattison *et al.*, 2003), and is traditionally the primary drawback of applying classic geothermobarometry to electron microprobe analyses of metamorphic minerals. Nevertheless, the Al content of orthopyroxene, or $y(\text{opx}) \equiv X_{\text{Al,M1(opx)}}$, has been recognised as perhaps the most effective means of recovering near-peak *P–T* estimates for granulite facies terranes, based on the relative immobility of Al compared with Fe and Mg in orthopyroxene during retrograde metamorphism (Harley & Green, 1982; Harley, 1984; Fitzsimons & Harley, 1994; Pattison & Bégin, 1994; Aranovich & Berman, 1997; Harley, 1998c; Moraes *et al.*, 2002; Pattison *et al.*, 2003). Some of the problems of 'classic' geothermobarometry have been removed with the development of the 'retrieval' technique in which Fe–Mg mineral compositions are re-adjusted to converge in *P–T* space with y(opx)–Fe–Mg *P–T* estimates (e.g. Pattison & Bégin, 1994; Fitzsimons & Harley, 1994; Pattison *et al.*, 2003). Earlier it was noted that most, but not all, peak *P–T* estimates (Table 1) lie inside the experimentally and thermodynamically derived stability limits for orthopyroxene–sillimanite–quartz assemblages (see Fig. 4b). However as there may be considerable uncertainty associated with (some of) these estimates, an alternative approach for estimating 'peak' *P–T* using pseudosections is outlined.

For a given bulk composition, calculated pseudosections provide a useful and internally consistent means with which to convey equilibrium mineral chemistry information, such as y(opx). Calculated pseudosections may therefore provide a complimentary and/or alternative method to the 'retrieval' technique. An advantage of calculated pseudosections is that y(opx) information is calculable as isopleth contours *within* the mineral assemblage field of interest (displayed in Figs 4 & 5), with the (variable) equilibrium X_{Mg} calculated at every location along the isopleth. Therefore 'peak' *P–T* estimates made on the basis of y(opx) contours are constrained by the preserved/inferred peak mineral assemblage which is delineated graphically in *P–T* space. The power of using pseudosections and y(opx) data to constrain 'peak' *P–T* conditions increases when y(opx) data from pseudosections of several similar or different rocks from a terrane are superimposed to define an overlapping region of maximum-preserved conditions within the peak assemblage fields (e.g. superimpose peak assemblage fields in Fig. 5c,d). Independent

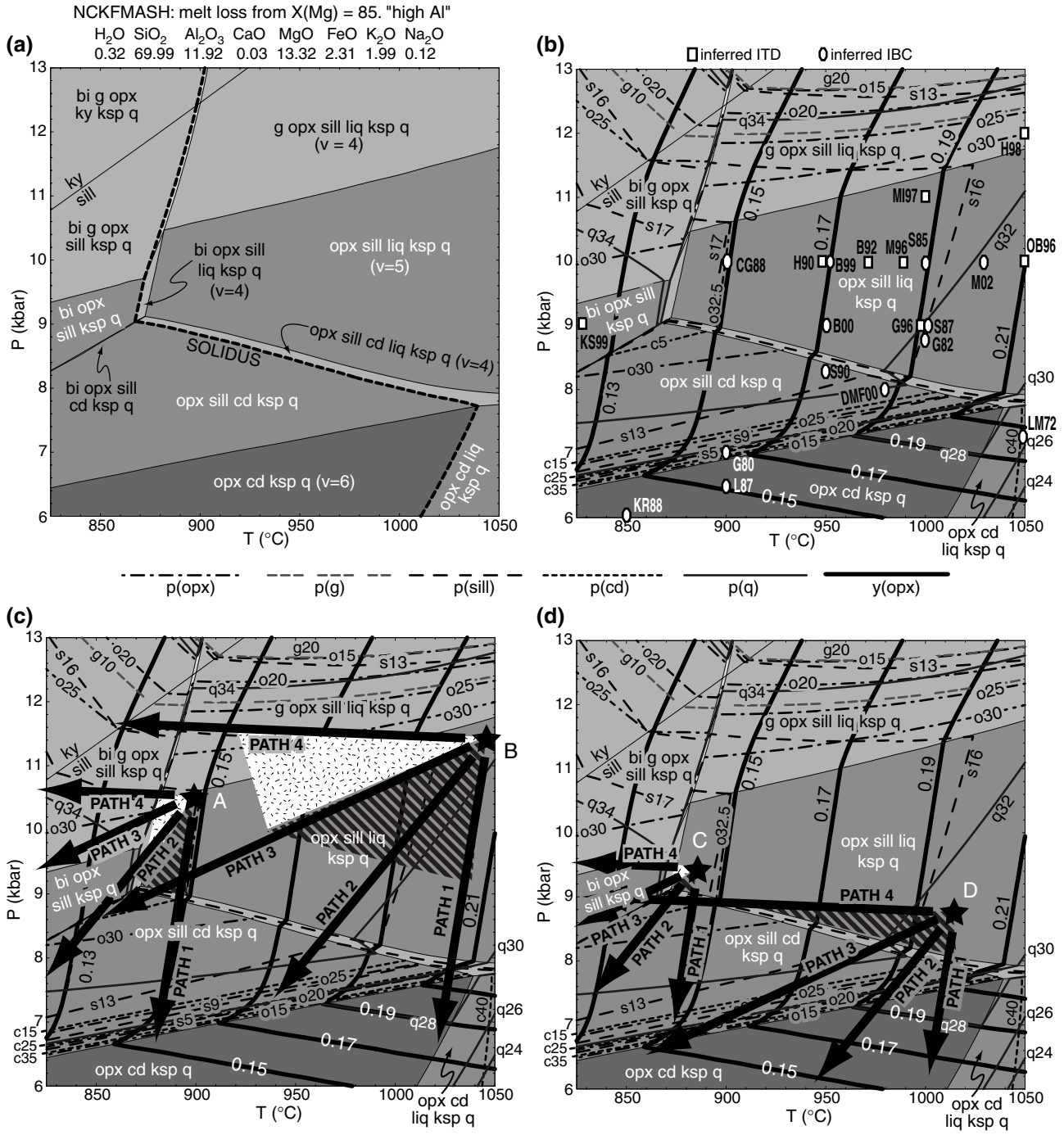

Fig. 4. An illustrative *P–T* pseudosection for a residual bulk composition resulting from progressive melt loss, approximated by melt loss events above the muscovite- and biotite-out melting steps from the (initial) composition in Fig. 3 (c). Melt loss event 1 involved loss of 90% of 13% melt at 780 °C, 10 kbar. Melt loss event 2 involved loss of 95% of 29% melt at 880 °C, 10 kbar. (a) Topology of assemblages in the now largely anhydrous bulk composition. Orthopyroxene and sillimanite remain stable together below the solidus (dashed line). A small (*c*. 2 molar percentage) amount of melt is present above the solidus. Assemblage variance, v, as indicated. (b) Mineral proportion (p(opx), etc. in legend; in molar percentage) and *y*(opx) information superimposed on the assemblage fields. *P–T* estimates for most orthopyroxene–sillimanite–quartz occurrences documented in Table 1 are also displayed. (c) and (d) depict an array of retrograde *P–T* paths emanating from four hypothetical peak *P–T* conditions (stars A to D). *P–T* Paths 1 through 4 are discussed in the text. White stippled regions encompass the range of d*P*/d*T* that will generate an inferred cooling texture, retrograde biotite. Obliquely striped regions encompass the range of d*P*/d*T* that will generate an inferred decompression texture, retrograde cordierite. ITD paths typically involve consumption of orthopyroxene, sillimanite and quartz. IBC paths may result in an increased abundance of quartz, and little change in orthopyroxene and sillimanite abundance.

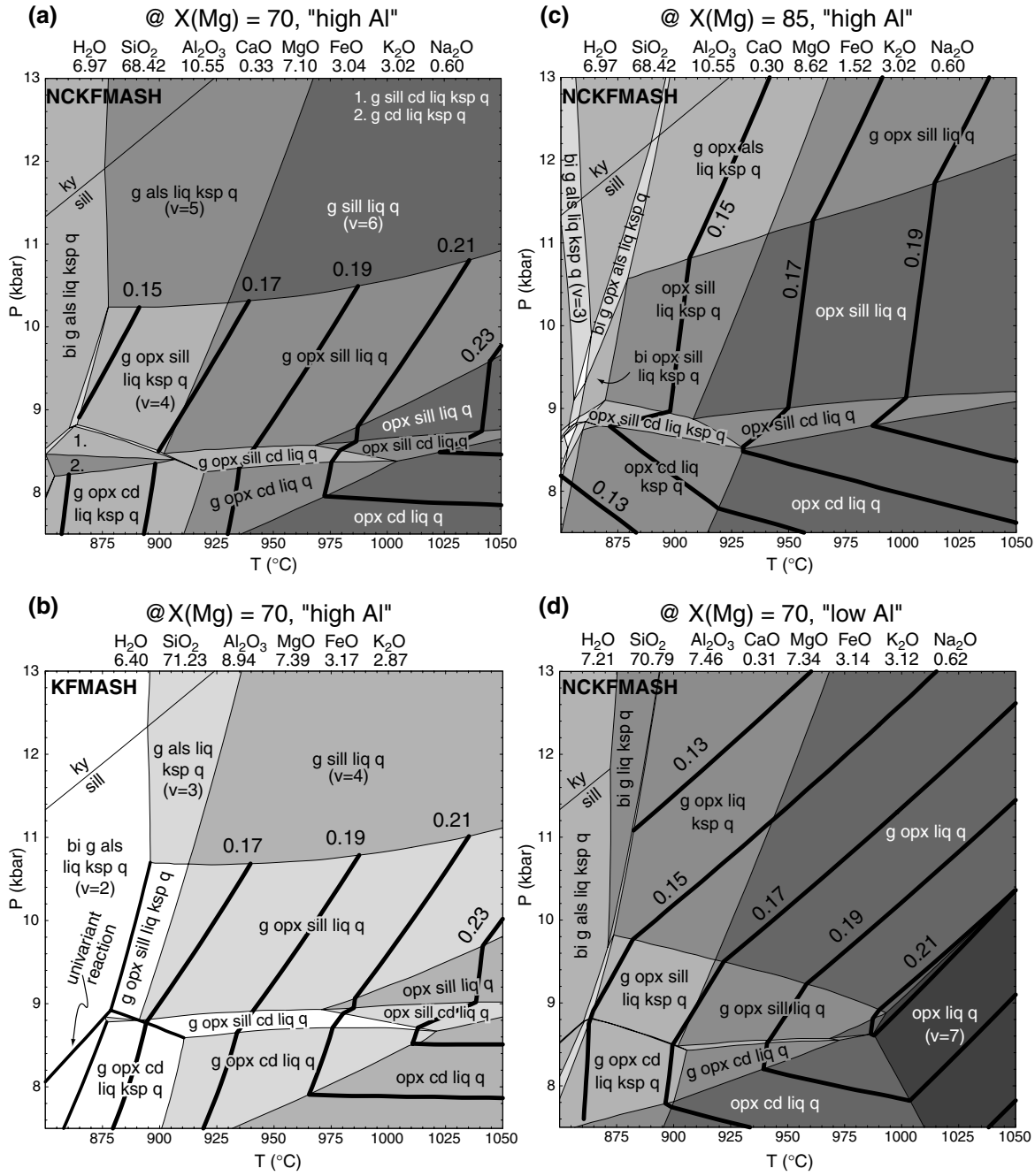

Fig. 5. Insets of *P–T* pseudosections from Fig. 3 showing *y*(opx) contours within high-*T* assemblage fields. Field variance shades are indicated in (a) and (b). A comparison of (c) with Fig. 4 indicates that as substantial melt loss has little impact on X_{Mg}, the *P–T* locus of a given *y*(opx) contour does not differ greatly between the two bulk compositions. Hence the contours in (a) – (d) may be used to broadly estimate 'peak' *P–T*.

petrographic evidence such as kyanite, exsolved metamorphic pyroxene (Sandiford & Powell, 1986; Harley, 1987) or mesoperthites (Sandiford, 1985; Hokada, 2001) may also provide useful constraints on the maximum possible limits of pressure and temperature in UHT terranes.

The *P–T* locations of individual *y*(opx) contours in Figs 4 and 5(c) are comparable within the peak orthopyroxene–sillimanite–quartz ± garnet ± K-feldspar field, as melt loss (affecting A/AFM) has little effect on the *P–T* location of a given *y*(opx) isopleth (compare also Fig. 5a,d). Rather, bulk X_{Mg} exerts a greater influence, such that more magnesian rocks have *less* aluminous orthopyroxene for a given *P–T* in the orthopyroxene + sillimanite + quartz + liquid ± garnet ± cordierite field (e.g. compare Fig. 5c with 5a

& d). Therefore the y(opx) contours in Fig. 5 could be used generally for the purpose of estimating 'peak' P–T for rocks of, or approximating, bulk $X_{Mg} = 70$ and 85, for both garnet-bearing and garnet-absent orthopyroxene–sillimanite–quartz occurrences. Therefore, in general, the pseudosection approach could be applied to refine and/or reassess the P–T estimates documented in Table 1. Most notably this would be appropriate for those estimates that lie outside the peak assemblages field(s) (e.g. Leong & Moore, 1972; Grew, 1980; Harris & Holland, 1984; Avakyan & Dmitriyeva, 1985; Lal *et al*., 1987; Kamineni & Rao, 1988; Kriegsman & Schumacher, 1999), but also those estimates already lying *within* the peak assemblage field (Fig. 4b). While this is beyond the scope of the paper, being able to appraise the accuracy/reliability of the P–T estimates in detail would require a greater knowledge of mineral proportions in the mineral assemblage(s), reflected in a more precise bulk composition, a consideration of other useful mineral reaction textures, and ideally the inclusion of sapphirine in phase diagram calculations.

Values of y(opx) from inferred ITD and IBC terranes typically range between *c*. 0.13 and 0.20 (Table 1). This suggestion of a wide range in P–T conditions is supported graphically by the spacing of y(opx) contours (Figs 4 & 5). A good fit of several P–T estimates from Table 1 with the pseudosections (Figs 4 & 5; Harley *et al*., 1990; Mouri *et al*., 1996; Ouzegane & Boumaza, 1996) may in fact indicate that these particular pseudosections are appropriate to these particular occurrences/samples. A lesser fit for most other occurrences whose P–T estimates nevertheless still plot within the orthopyroxene–sillimanite–quartz field may indicate the illustrative pseudosections have a slightly inappropriate bulk composition to be directly applicable.

POSSIBILITIES FOR *P–T* PATH TRAJECTORIES

There is a tendency for the retrograde P–T paths of UHT granulite facies terranes to be classified as either ITD or IBC (Table 1). With reference to Fig. 4, this section explores the possibilities for P–T path interpretations on the basis of inferred mineral reaction textures in orthopyroxene–sillimanite–quartz rocks, citing examples from Table 1. This discussion will concentrate on terranes in which ITD has been invoked, where cordierite is observed to be a common product of peak orthopyroxene–sillimanite–quartz breakdown in sapphirine-absent rocks.

Figure 4(c,d) shows a range of P–T trajectories from different hypothetical peak conditions (marked by stars A through D). Paths 1 through 4 have identical respective dP/dT for each scenario A through D. Each path conveys a hypothetical *initial* postpeak vector of the P–T path experienced by a granulite facies rock, and does not imply that the P–T path will remain as shown throughout the entire retrograde/exhumation history. Path 1 represents a near-ITD path, whereas Path 4 represents a near-IBC path.

From each peak P–T location in Fig. 4(c,d), there is a range of possible P–T paths that pass through the narrow cordierite-liquid-bearing stability field (i.e. the solidus) to facilitate the growth of cordierite coronas (obliquely striped regions), initially in the presence of melt. The range of dP/dT that cross into the cordierite-bearing fields is a strong function of the peak P–T condition. Thus, a potentially wide range of dP/dT retrograde P–T paths may be able to generate a cordierite-bearing mineral reaction texture generally ascribed only to ITD P–T paths. Moreover, P–T paths from Peak D (Fig. 4d) demonstrate that the onset of cordierite growth does not necessarily imply large amounts of decompression from peak conditions. Depending on the peak P–T, retrograde cordierite may be a cooling product (IBC). Therefore, a mineral reaction texture in isolation is unlikely to uniquely define a retrograde P–T path (Vernon, 1996; Brown, 2002). The extent of cordierite growth along each of Paths 1–4, and the morphology of the reaction texture (e.g. corona v. symplectite, grain size, grain distribution), will likely depend additionally upon other factors such as dP/dt and dT/dt. However, with knowledge of peak P–T, calculated pseudosections can quantify the amount of decompression (or cooling) required to initiate the growth of an observed mineral reaction texture. For example, where retrograde cordierite coronas are developed in interpreted high-pressure terranes (Fig. 4b; Rauer Group: H98, Harley, 1998b; Lützow-Holm Bay: MI97 Motoyoshi & Ishikawa, 1997; South Harris: B99 Baba, 1999), the retrograde P–T path must involve a substantial amount of decompression. In contrast, there is less need for a large amount of decompression to generate retrograde cordierite in terranes having experienced lower interpreted peak pressure, as for example at Forefinger Point, Antarctica (Harley *et al*., 1990).

Applying the same logic as for cordierite, a range of P–T paths instead encounter the lower-temperature biotite-bearing stability fields, again largely being a function of the peak P–T conditions (white stippled regions in Fig. 4c,d). The presence of retrograde biotite and its relationship to mineral reaction textures is important. However, depicting biotite via pseudosections is currently hampered by the stabilising effect of components not considered in the (NC)KFMASH system (e.g. Ti, F, Fe^{3+} Nair & Chacko, 2002). However, Harris & Holland (1984), Harley *et al*. (1990), Mouri *et al*. (1996), Ouzegane & Boumaza (1996), Harley (1998b) and Kriegsman & Schumacher (1999) indicate the presence of biotite in the orthopyroxene–sillimanite–quartz-bearing rocks. In theory if it can be deduced that the origin of the biotite can be attributed to the same implicit metamorphic cycle as the cordierite-bearing orthopyroxene–sillimanite–quartz assemblages, the presence of biotite may help to more uniquely define possible retrograde P–T path trajectories.

In general, the development of a particular retrograde mineral reaction texture in (high-grade) metamorphic rocks may be summarised as a function of several factors: (1) the peak metamorphic conditions, and where the peak *P–T* lies with respect to the boundaries of the peak assemblage field; (2) the retrograde *P–T* trajectory from peak conditional; (3) the first encountered lower-variance field involving significant mineral proportion changes that the rock enters along its retrograde path; (4) the proportion of melt remaining in the equilibration volume; and (5) the exhumation and/or cooling rate associated with the path.

Changes in mineral composition (e.g. *y*(opx)) and proportion within and across assemblage fields may be useful for constraining the locus of a *P–T* path (Stüwe & Powell, 1995), thereby providing a potential means of characterising and delineating between *P–T* paths 1–4, for example. The logic, here based on *y*(opx) and mineral proportion changes in orthopyroxene–sillimanite–quartz assemblages, is applicable to any mineral assemblage.

In Fig. 4(c,d), ITD *P–T* Path 1 tracks more or less parallel to the trend of *y*(opx) contours until reaching subsolidus conditions. Therefore a more or less homogeneous *y*(opx) profile core to rim may be expected (e.g. reported in high-grade textures by Harley *et al.*, 1990; Mouri *et al.*, 1996; Harley, 1998b; Bose *et al.*, 2000; Moraes *et al.*, 2002). Conversely, IBC *P–T* Path 4 involves crossing *y*(opx) contours steeply and in a decreasing trend. Therefore a markedly decreasing *y*(opx) profile may be expected from core to rim (possibly for high-grade assemblages in Lal *et al.*, 1987).

Decompression-dominated retrograde *P–T* paths (e.g. Paths 1–2, Fig. 4c,d) typically steeply cross mineral proportion contours, particularly from garnet-bearing peak conditions. Conversely, cooling-dominated retrograde *P–T* paths (e.g. Paths 3–4, Fig. 4c,d) cross proportion contours more shallowly from peak conditions. Generally the most profound mineral proportion change for a given change in *P–T* will occur as assemblage variance decreases with the growth of a new mineral (e.g. across narrow solidus fields, Fig. 4a). Unfortunately, the interplay of factors such as the effect of melt loss on kinetics (particularly at subsolidus conditions), d*P*/d*t* and d*T*/d*t*, and the temperature–time-dependent nature of an equilibration volume (Stüwe, 1997), render it difficult to match exact calculated mineral proportions (molar percentage) with those observed in thin section. Therefore, distinguishing between, say, Paths 1 and 3 from peak D (Fig. 5d), on the basis of matching calculated with observed mineral proportions would likely prove difficult. Fortunately, mineral proportion change during the retrograde evolution is useful in a *relative* sense if used in conjunction with other information. Therefore, as for estimating 'peak' *P–T* conditions, retrograde *P–T* path derivation using the calculated pseudosection approach should be integrative, integrating the petrography (i.e. assemblage(s) plus interpreted mineral proportion changes through retrograde reaction) with mineral chemistry and equilibration volume composition for many reaction textures from rocks of differing bulk composition. Employing these integrative tactics could be used, for example, to assess the *P–T* paths of inferred ITD and IBC terranes in Table 1 given the appropriate minerals can be modelled (e.g. sapphirine).

'End-member' *P–T* paths (ITD, IBC) as determined via the use of qualitative and/or semiquantitative *P–T* grids, while possibly appropriate for several localities, are not necessarily appropriate for the interpretation of many UHT granulite facies terranes. If either 'end-member' *P–T* path is to be invoked, one must be wary of the possible associated tectonic implications. *P–T* Path 1 (ITD) in Fig. 4 implies terrane exhumation significantly more rapid than decay of the thermal perturbation causing metamorphism. On the other hand, *P–T* Path 4 (IBC) implies little or no exhumation associated with the decay of the thermal perturbation, and may be indicative of crust in isostatic equilibrium (Sandiford, 1985). A low d*T*/d*t* potentially associated with IBC paths may be highlighted by the growth of 'late' kyanite and cordierite in some inferred IBC rocks (Table 1). Since metamorphic pressures responsible for the generation of orthopyroxene–sillimanite–quartz assemblages in UHT terranes are not necessarily indicative of greatly overthickened crust (e.g. Sandiford, 1985; Sandiford, 1989), the driving mechanism inherently associated with particularly ITD-type *P–T* paths must be addressed. In addition, the ultimate mechanism for exhumation of UHT granulites may not be tectonically related to the UHT metamorphic process (Sandiford, 1985; Ellis, 1987; Sandiford, 1989). Therefore the interpretation of *P–T* paths in UHT rocks as ITD or IBC may be overly simplistic as mineral reaction textures rarely define a unique *P–T* path. Failing to realise all the *P–T* path possibilities from a suite of mineral reaction textures may have severe implications for interpretations of the tectonic setting and evolution of a terrane.

CONCLUSION

Preserved high-grade mineral assemblages such as orthopyroxene–sillimanite–quartz are useful indicators of lower crustal conditions. Whilst the discussion regarding assemblage preservation and *P–T* paths is focussed on orthopyroxene–sillimanite–quartz assemblages, the logic is applicable to textural development in other metamorphic rocks. Since a mineral reaction texture does not uniquely define a *P–T* path, the common interpretation of retrograde *P–T* paths in high-grade rocks as ITD or IBC may be overly simplistic. Therefore, the constraining of a retrograde *P–T* path in high-grade rocks, which invariably has an impact on tectonic models, should be derived via an integrative approach. Calculated pseudosections provide a graphical and internally consistent means of expressing the

assemblage, chemical and mineral proportion information for a specified bulk composition, thereby allowing for the integration of information from many similar or different mineral reaction textures from a given locality. Therefore the pseudosection approach may provide a powerful alternative and/or compliment to other thermobarometric techniques.

ACKNOWLEDGEMENTS

The motivation for this study was provided by samples collected during fieldwork in the Rauer Group, east Antarctica, during the 1999–2000 and 2000–01 austral summers. Antarctic fieldwork was carried out under the guise of ASAC Project 1129, awarded to Professor C. Wilson. T. Chacko, M. Guiraud and T. Johnson are thanked for constructive reviews. DEK is supported by an Australian Postgraduate Award. RWW was supported by ARC Discovery Project DPO209461.

REFERENCES

Annersten, H. & Seifert, F., 1981. Stability of the assemblage orthopyroxene-sillimanite-quartz in the system MgO-FeO-Fe_2O_3-Al_2O_3-SiO_2-H_2O. *Contributions to Mineralogy and Petrology*, **77,** 158–165.

Anovitz, L. M., 1991. Al zoning in pyroxene and plagioclase: Window on late prograde to early retrograde *P-T* paths in granulite terrains. *American Mineralogist*, **76,** 1328–1343.

Aranovich, L., Ya. & Berman, R. G., 1997. A new garnet-orthopyroxene thermometer based on reversed Al_2O_3 solubility in FeO-Al_2O_3-SiO_2 orthopyroxene. *American Mineralogist*, **82,** 345–353.

Ashworth, J. R., 1993. Fluid-absent diffusion kinetics of Al inferred from retrograde metamorphic coronas. *American Mineralogist*, **78,** 331–337.

Audibert, N., Hensen, B. J. & Bertrand, P., 1995. Experimental study of phase relations involving osumilite in the system K_2O-FeO-MgO-Al_2O_3-SiO_2-H_2O at high pressure and temperature. *Journal of Metamorphic Geology*, **13,** 331–344.

Avakyan, K. K. & Dmitriyeva, M. T., 1985. Orthopyroxene-sillimanite-sapphirine assemblages in charnockitic gneisses of the central Kola Peninsula. *International Geology Review*, **27,** 1465–1469.

Baba, S., 1999. Sapphirine-bearing orthopyroxene-kyanite/sillimanite granulites from South Harris, NW Scotland: evidence for Proterozoic UHT conditions in the Lewisian. *Contributions to Mineralogy and Petrology*, **136,** 33–47.

Bertrand, P., Ouzegane, Kh & Kienast, J. R., 1992. *P-T-X* relationships in the Precambrian Al-Mg-rich granulites from In Ouzzal, Hoggar, Algeria. *Journal of Metamorphic Geology*, **10,** 17–31.

Bose, S., Fukuoka, M., Sengupta, P. & Dasgupta, S., 2000. Evolution of high-Mg-Al granulites from Sunkarametta, Eastern Ghats, India: evidence for a lower crustal heating – cooling trajectory. *Journal of Metamorphic Geology*, **18,** 223–240.

Brown, M., 1994. The generation, segregation, ascent and emplacement of granite magma: the migmatite-to-crustally-derived granite connection in thickened orogens. *Earth-Science Reviews*, **36,** 83–130.

Brown, M., 2002. Retrograde processes in migmatites and granulites revisited. *Journal of Metamorphic Geology*, **20,** 25–40.

Brown, M., Averkin, Y., McLellan, E. & Sawyer, E., 1995. Melt segregation in migmatites. *Journal of Geophysical Research*, **100,** 15 655–15 679.

Brown, M. & Rushmer, T., 1997. The role of deformation in the movement of granite melt: views from the laboratory and the field. In: *Deformation-Enhanced Fluid Transport in the Earth's Crust and Mantle, The Mineralogical Society Series 8*, (ed. Holness, M. B.), pp. 111–144. Chapman & Hall, London.

Brown, M. & Solar, G., 1998. Granite ascent and emplacement during contractional deformation in convergent orogens. *Journal of Structural Geology*, **20,** 1365–1393.

Carrington, D. P., 1995. The relative stability of garnet-cordierite and orthopyroxene-sillimanite-quartz assemblages in metapelitic granulites: experimental data. *European Journal of Mineralogy*, **7,** 949–960.

Carrington, D. P. & Harley, S. L., 1995. Partial melting and phase relations in high-grade metapelites: an experimental petrogenetic grid in the KFMASH system. *Contributions to Mineralogy and Petrology*, **120,** 270–291.

Chinner, G. A. & Sweatman, T. R., 1968. A former association of enstatite and kyanite. *Mineralogical Magazine*, **36,** 1052–1060.

Clarke, G. L. & Powell, R., 1991. Decompressional coronas and symplectites in granulites of the Musgrave Complex, central Australia. *Journal of Metamorphic Geology*, **9,** 441–450.

Clarke, G. L., Powell, R. & Guiraud, M., 1989. Low-pressure granulite facies metapelitic assemblages and corona textures from MacRobertson Land, east Antarctica: the importance of Fe_2O_3 and TiO_2 in accounting for spinel-bearing assemblages. *Journal of Metamorphic Geology*, **7,** 323–335.

Currie, K. L. & Gittins, J., 1988. Contrasting sapphirine parageneses from Wilson Lake, Labrador and their tectonic implications. *Journal of Metamorphic Geology*, **6,** 603–622.

Dasgupta, S., Sengupta, P., Ehl, J., Raith, M. & Bardhan, S., 1995. Reaction Textures in a Suite of Spinel Granulites from the Eastern Ghats Belt, India: Evidence for Polymetamorphism, a Partial Petrogenetic Grid in the System KFMASH and the Roles of ZnO and Fe_2O_3. *Journal of Petrology*, **36,** 435–461.

Droop, G. T. R., 1989. Reaction history of garnet-sapphirine granulites and conditions of Archaean high-pressure granulite facies metamorphism in the Central Limpopo Mobile Belt, Zimbabwe. *Journal of Metamorphic Geology*, **7,** 383–403.

Droop, G. T. R. & Bucher-Nurminen, K., 1984. Reaction textures and metamorphic evolution of sapphirine-bearing granulites from the Gruf complex, Italian Central Alps. *Journal of Petrology*, **25,** 766–803.

Ellis, D. J., 1987. Origin and evolution of granulites in normal and thickened crusts. *Geology*, **15,** 167–170.

Ellis, D. J., Sheraton, J. W., England, R. N. & Dallwitz, W. B., 1980. Osumilite-sapphirine-quartz granulites from Enderby Land, Antarctica: mineral assemblages and reactions. *Contributions to Mineralogy and Petrology*, **72,** 123–143.

Fitzsimons, I. C. W. & Harley, S. L., 1994. The Influence of Retrograde Cation Exchange on Granulite *P-T* Estimates and a Convergence Technique for the Recovery of Peak Metamorphic Conditions. *Journal of Petrology*, **35,** 543–576.

Frost, B. R. & Chacko, T., 1989. The granulite uncertainty principle: limitations on thermobarometry in granulites. *Journal of Geology*, **97,** 435–450.

Fyfe, W. S., 1973a. The granulite facies, partial melting and the Archaean crust. *Philosophical Transactions of the Royal Society of London, Series A. Mathematical and Physical Sciences*, **247,** 457–461.

Fyfe, W. S., 1973b. The generation of batholiths. *Tectonophysics*, **17,** 273–283.

Grant, J. A., 1985. Phase equilibria in partial melting of pelitic rocks. In: *Migmatites* (ed. Ashworth, J. R.), pp. 86–144, Blackie, Glasgow.

Grew, E. S., 1982. Osumilite in the sapphirine-quartz terrane of Enderby Land, Antarctica: implications for osumilite petrogenesis in the granulite facies. *American Mineralogist*, **67,** 762–787.

Grew, E. S., 1980. Sapphirine + quartz association from Archean rocks in Enderby Land, Antarctica. *American Mineralogist*, **65,** 821–836.

Guiraud, M., Kienast, J. R. & Rahmani, A., 1996. Petrological study of high-temperature granulites from In Ouzzal, Algeria: some implications on the phase relationships in the FMASTOCr system. *European Journal of Mineralogy*, **8,** 1375–1390.

Guiraud, M., Powell, R. & Rebay, G., 2001. H_2O in metamorphism and unexpected behaviour in the preservation of metamorphic mineral assemblages. *Journal of Metamorphic Geology*, **19,** 445–454.

Hand, M. & Dirks, P. H. G. M., 1992. The influence of deformation on the formation of axial-planar leucosomes and the segregation of small melt bodies within the migmatitic Napperby Gneiss, central Australia. *Journal of Structural Geology*, **14,** 591–604.

Harley, S. L., 1984. The solubility of alumina in orthopyroxene coexisting with garnet in FeO-MgO-Al_2O_3-SiO_2 and CaO-FeO-MgO-Al_2O_3-SiO_2. *Journal of Petrology*, **25,** 665–696.

Harley, S. L., 1987. A pyroxene-bearing metaironstone and other pyroxene-granulites from Tonagh Island, Enderby Land, Antarctica: further evidence for very high temperature (>980 °C) Archaean regional metamorphism in the Napier Complex. *Journal of Metamorphic Geology*, **5,** 341–356.

Harley, S. L., 1998a. On the occurrence and characterisation of ultrahigh-temperature (UHT) crustal metamorphism. In: *What Drives Metamorphic Reactions? Special Publication 138*, (eds Treloar, P. J. &. O'Brien, P.), pp. 75–101. The Geological Society, London.

Harley, S. L., 1998b. Ultrahigh temperature granulite metamorphism (1050 °C, 12 kbar) and decompression in garnet (Mg70)-orthopyroxene-sillimanite gneisses from the Rauer Group, East Antarctica. *Journal of Metamorphic Geology*, **16,** 541–562.

Harley, S. L., 1998c. An Appraisal of Peak Temperatures and Thermal Histories In Ultrahigh-Temperature (UHT) Crustal Metamorphism: The Significance of Aluminous Orthopyroxene. *Memoirs of the National Institute of Polar Research, Special Issue*, **53,** 49–73.

Harley, S. L. & Fitzsimons, I. C. W., 1991. Pressure-temperature evolution of metapelitic granulites in a polymetamorphic terrane: the Rauer Group, East Antarctica. *Journal of Metamorphic Geology*, **9,** 231–243.

Harley, S. L. & Green, D. H., 1982. Garnet-orthopyroxene barometry for granulites and peridotites. *Nature*, **300,** 697–701.

Harley, S. L., Hensen, B. J. & Sheraton, J. W., 1990. Two-stage decompression in orthopyroxene-sillimanite granulites from Forefinger Point, Enderby Land, Antarctica: implications for the evolution of the Archaean Napier Complex. *Journal of Metamorphic Geology*, **8,** 591–613.

Harris, N. B. W. & Holland, T. J. B., 1984. The significance of cordierite-hypersthene assemblages from the Beitbridge region of the Central Limpopo belt: evidence for rapid decompression in the Archean? *American Mineralogist*, **69,** 1036–1049.

Hensen, B. J., 1971. Theoretical Phase Relations Involving Cordierite and Garnet in the System MgO-FeO-Al_2O_3-SiO_2. *Contributions to Mineralogy and Petrology*, **33,** 191–214.

Hensen, B. J., 1986. Theoretical phase relations involving cordierite and garnet revisited: the influence of oxygen fugacity on the stability of sapphirine and spinel in the system Mg-Fe-Al-Si-O. *Contributions to Mineralogy and Petrology*, **92,** 362–367.

Hensen, B. J., 1987. *P-T* grids for silica-undersaturated granulites in the systems MAS ($n+4$) and FMAS ($n+3$) – tools for the derivation of *P-T* paths of metamorphism. *Journal of Metamorphic Geology*, **5,** 255–271.

Hensen, B. J. & Harley, S. L., 1990. Graphical analysis of *P-T-X* relations in granulite facies metapelites. In: *High-Temperature Metamorphism and Crustal Anatexis, The Mineralogical Society of Great Britain, Series 2*, (eds Ashworth, J. R. & Brown, M.), pp. 19–56. Unwin-Hyman, London.

Hensen, B. J. & Osanai, Y., 1994. Experimental study of dehydration melting of F-bearing biotite in model pelitic compositions. *Mineralogical Magazine*, **58A,** 410–411.

Hokada, T., 2001. Feldspar thermometry in ultrahigh-temperature metamorphic rocks: Evidence of crustal metamorphism attaining ~1100 °C in the Archean Napier Complex, East Antarctica. *American Mineralogist*, **86,** 932–938.

Johnson, T. E., Gibson, R. L., Brown, M., Buick, I. S. & Cartwright, I., 2003. Partial melting of metapelitic rocks beneath the Bushveld Complex, South Africa. *Journal of Petrology*, **44,** 789–813.

Kamineni, D. C. & Rao, A. T., 1988. Sapphirine-bearing quartzite from the Eastern Ghats terrain, Vizianagaram, India. *Journal of Geology*, **96,** 209–220.

Kelly, N. M., Clarke, G. L. & Fanning, C. M., 2002. A two-stage evolution of the Neoproterozoic Rayner Structural Episode: new U-Pb sensitive high resolution ion microprobe constraints from the Oygarden Group, Kemp Land, East Antarctica. *Precambrian Research*, **116,** 307–330.

Kriegsman, L. M. & Schumacher, J. C., 1999. Petrology of Sapphirine-bearing and Associated Granulites from Central Sri Lanka. *Journal of Petrology*, **40,** 1211–1239.

Lal, R. K., Ackermand, D., Seifert, F. & Haldar, S. K., 1978. Chemographic relationships in sapphirine-bearing rocks from Sonapahar, Assam, India. *Contributions to Mineralogy and Petrology*, **67,** 169–187.

Lal, R. K., Ackermand, D. & Upadhyay, H., 1987. *P-T-X* relationships deduced from corona textures in sapphirine-spinel-quartz assemblages from Paderu, southern India. *Journal of Petrology*, **28,** 1139–1169.

Leong, K. M. & Moore, J. M., 1972. Sapphirine-bearing rocks from Wilson Lake, Labrador. *Canadian Mineralogist*, **11,** 777–790.

McDade, P. & Harley, S. L., 2001. A petrogenetic grid for aluminous granulite facies metapelites in the {KFMASH} system. *Journal of Metamorphic Geology*, **19,** 45–59.

Moraes, R., Brown, M., Fuck, R. A., Camargo, M. A. & Lima, T. M., 2002. Characterisation and *P-T* Evolution of Melt-bearing Ultrahigh-temperature Granulites: an Example from the Anápolis – Itauçu Complex of the Brasília Fold Belt, Brazil. *Journal of Petrology*, **43,** 1673–1705.

deMoraes, R. & Fuck, R. A., 2000. Ultra-high-temperature metamorphism in Central Brazil: the Barro Alto complex. *Journal of Metamorphic Geology*, **18,** 345–358.

Morse, S. A. & Talley, J. H., 1971. Sapphirine reactions in deep-seated granulites near Wilson Lake, Central Labrador, Canada. *Earth and Planetary Science Letters*, **10,** 325–328.

Motoyoshi, Y. & Ishikawa, M., 1997. Metamorphic and structural evolution of granulites from Rundvågshetta, Lützow-Holm Bay, East Antarctica. In: *The Antarctic Region: Geological Evolution and Processes* (ed. Ricci, C. A.), pp. 65–72. Terra Antarctica Publications, Suna.

Mouri, H., Guiraud, M. & Hensen, B. J., 1996. Petrology of phlogopite-sapphirine-bearing Al-Mg granulites from Ihouhaouene, In Ouzzal, Hoggar, Algeria: an example of phlogopite stability at high temperature. *Journal of Metamorphic Geology*, **14,** 725–738.

Nair, R. & Chacko, T., 2002. Fluid-absent melting of high-grade semipelite: *P-T* constraints on orthopyroxene formation and implications for granulite genesis. *Journal of Petrology*, **43,** 2121–2142.

O'Hara, M. J., 1977. Thermal history of excavation of Archaean gneisses from the base of the continental crust. *Journal of the Geological Society, London*, **134,** 185–200.

Ouzegane, K. & Boumaza, S., 1996. An example of ultra-high-temperature metamorphism: orthopyroxene-sillimanite-garnet, sapphirine-quartz and spinel-quartz parageneses in Al-Mg granulites from In Hihaou, In Ouzzal, Hoggar. *Journal of Metamorphic Geology*, **14,** 693–708.

Pattison, D. R. M. & Bégin, N. J., 1994. Zoning patterns in orthopyroxene and garnet in granulites: implications for

geothermometry. *Journal of Metamorphic Geology*, **12,** 387–410.

Pattison, D. R. M., Chacko, T., Farquhar, J. & McFarlane, C. R. M., 2003. Temperatures of granulite-facies metamorphism: constraints from experimental phase equilibria and thermobarometry corrected for retrograde exchange. *Journal of Petrology*, **44,** 867–900.

Peterson, J. W., Chacko, T. & Kuehner, S. M., 1991. The effect of fluorine on the vapor-absent melting of phlogopite + quartz: implication for deep-crustal processes. *American Mineralogist*, **76,** 470–476.

Powell, R., 1983. Processes in Granulite-facies Metamorphism. In: *Migmatites, Melting and Metamorphism* (eds Atherton, M. P. & Gribble, C. D.), pp. 127–139. Shiva Publishing, Nantwich.

Powell, R. & Downes, J., 1990. Garnet porphyroblast-bearing leucosomes in metapelites: mechanisms, phase diagrams, and an example from Broken Hill, Australia. In: *High-Temperature Metamorphism and Crustal Anatexis, The Mineralogical Society of Great Britain, Series 2*, (eds Ashworth, J. R. & Brown, M.), pp. 105–123. Unwin-Hyman, London.

Powell, R. & Holland, T. J. B., 1988. An internally consistent thermodynamic dataset with uncertainties and correlations: 3. Application methods, worked examples and a computer program. *Journal of Metamorphic Geology*, **6,** 173–204.

Powell, R. & Sandiford, M., 1988. Sapphirine and spinel phase relationships in the system FeO-MgO-Al_2O_3-SiO_2-TiO_2-O_2. *Contributions to Mineralogy and Petrology*, **98,** 64–71.

Raith, M., Karmakar, S. & Brown, M., 1997. Ultra-high-temperature metamorphism and multistage decompressional evolution of sapphirine granulites from the Palni Hills Ranges, southern India. *Journal of Metamorphic Geology*, **15,** 379–399.

Rickers, K., Raith, M. & Dasgupta, S., 2001. Multistage reaction textures in xenolithic high-MgAl granulites at Anakapelle, Eastern Ghats Belt, India: examples of contact polymetamorphism and infiltration-driven metasomatism. *Journal of Metamorphic Geology*, **19,** 563–582.

Rubie, D. C., 1986. The catalysis of mineral reactions by water and restrictions on the presence of aqueous fluid during metamorphism. *Mineralogical Magazine*, **50,** 399–415.

Rutter, E. H., 1997. The influence of deformation on the extraction of crustal melts: a consideration of the role of melt-assisted granular flow. In: *Deformation-Enhanced Fluid Transport in the Earth's Crust and Mantle, Series 8, The Mineralogical Society*, (ed. Holness, M. B.), pp. 82–110. Chapman & Hall, London.

Sandiford, M., 1985. The metamorphic evolution of granulites at Fyfe Hills; implications for Archaean crustal thickness in Enderby Land, Antarctica. *Journal of Metamorphic Geology*, **3,** 155–178.

Sandiford, M., 1989. Horizontal structures in granulite terrains: a record of mountain building or mountain collapse? *Geology*, **17,** 449–452.

Sandiford, M., Neall, F. B. & Powell, R., 1987. Metamorphic evolution of aluminous granulites from Labwor Hills, Uganda. *Contributions to Mineralogy and Petrology*, **95,** 217–225.

Sandiford, M. & Powell, R., 1986. Pyroxene exsolution in granulites from Fyfe Hills, Enderby Land, Antarctica: Evidence for 1000 °C metamorphic temperatures in Archean continental crust. *American Mineralogist*, **71,** 946–954.

Sarkar, A., Bhanumathi, L. & Balasubrahmanyan, M. N., 1981. Petrology, geochemistry and geochronology of the Chilka Lake igneous complex, Orissa state, India. *Lithos*, **14,** 93–111.

Sawyer, E. W., 1994. Melt segregation in the continental crust. *Geology*, **22,** 1019–1022.

Sawyer, E. W., Dombrowski, C. & Collins, W. J., 1999. Movement of melt during synchronous regional deformation and granulite-facies anatexis, an example from the Wuluma Hills, central Australia. In: *Understanding Granites: Integrating New and Classical Techniques, Special Publication 158*, (eds Castro, A., Fernandez, C. & Vigneresse, J-L.), pp. 221–237. Geological Society, London.

Sengupta, P., Dasgupta, S., Battacharya, P. K., Fukuoka, M., Chakraborti, S. & Bhowmick, S., 1990. Petro-tectonic Imprints in the Sapphirine Granulites from Anantagiri, Eastern Ghats Mobile Belt, India. *Journal of Petrology*, **31,** 971–996.

Spear, F. S., 1993. *Metamorphic Phase Equilibria and Pressure-Temperature-Time Paths*. Mineralogical Society of America, Washington DC.

Stüwe, K., 1997. Effective bulk composition changes due to cooling: a model predicting complexities in retrograde reaction textures. *Contributions to Mineralogy and Petrology*, **129,** 43–52.

Stüwe, K. & Powell, R., 1995. *P-T* Paths from modal proportions: application to the Koralm Complex, Eastern Alps. *Contributions to Mineralogy and Petrology*, **119,** 83–93.

Vanderhaeghe, O., 2001. Melt segregation, Pervasive Melt Migration and Magma Mobility in the Continental Crust: The Structural Record from Pores to Orogens. *Physics and Chemistry of the Earth, Part A*, **26,** 213–223.

Vernon, R. H., 1996. Problems with inferring *P-T-t* paths in low-*P* granulite facies rocks. *Journal of Metamorphic Geology*, **14,** 143–153.

Waters, D. J., 1986. Metamorphic History of Sapphirine-bearing and Related Magnesian Gneisses from Namaqualand, South Africa. *Journal of Petrology*, **27,** 541–565.

Waters, D. J., 1988. Partial melting and the formation of granulite facies assemblages in Namaqualand, South Africa. *Journal of Metamorphic Geology*, **6,** 387–404.

White, R. W. & Powell, R., 2002. Melt loss and the preservation of granulite facies mineral assemblages. *Journal of Metamorphic Geology*, **20,** 621–632.

White, R. W., Powell, R. & Clarke, G. L., 2002. The interpretation of reaction textures in Fe-rich metapelitic granulites of the Musgrave Block, central Australia: constraints from mineral equilibria calculations in the system K_2O-FeO-MgO-Al_2O_3-SiO_2-H_2O-TiO_2-Fe_2O_3. *Journal of Metamorphic Geology*, **20,** 41–55.

White, R. W., Powell, R. & Holland, T. J. B., 2001. Calculation of partial melting equilibria in the system Na_2O-CaO-K_2O-FeO-MgO-Al_2O_3-SiO_2-H_2O (NCKFMASH). *Journal of Metamorphic Geology*, **19,** 139–153.

Wickham, S. M., 1987. The segregation and emplacement of granitic magmas. *Journal of the Geological Society, London*, **144,** 281–297.

Yund, R. A., 1997. Rates of grain boundary migration diffusion through enstatite and forsterite reaction rims. *Contributions to Mineralogy and Petrology*, **126,** 224–236.

Received 12 September 2002; revision accepted 23 February 2003.